Integrated stratigraphy from a transgressive upper Oligocene section in NW Italy

Antonino Briguglio, Simone Crobu, Eleni Lutaj and Michele Piazza
DISTAV, Unversità degli Studi di Genova, Corso Europa 26, 16132 Genova, Italy
email: antonino.briguglio@unige.it

ABSTRACT: The Oligo-Miocene Transition (OMT) is one of the most important climatic transitions of the last 30 million years. This short period of climate warming coincides with a few biotic turnovers, which are well known in deeper marine settings where stratigraphic successions yield a detailed record; in shallow marine environments they have been proved difficult to recognize as the occurrence and absence of certain taxa due to ecological preferences hamper the study. This study focuses on the Case Cné section in the late Oligocene of the Tertiary Piedmont Basin (TPB) as it represents a gradual transgressive event, which shows the drowning of a locally developed reef complex and development of a deeper marine sedimentary setting influenced by gravity flow mechanics. Larger foraminifera biostratigraphy was used to date the section to the late Oligocene (SBZ23); preliminary strontium isotope data confirms this result. Using sedimentological, semi-quantitative microfacies and geochemical analysis the sedimentary history of the section was reconstructed and divided into four major phases: the drowning of the reef complex, a short prograding phase of the fluvial system, the onset of gravity flow mechanics and a final transgressive phase with an initial turbiditic influence which continues regionally into the Miocene.

Keywords: Gamma Ray, foraminifera, warming event, Cenozoic

INTRODUCTION

The Oligo- Miocene Transition is widely regarded as one of the most important climate transitions in the Cenozoic and is generally interpreted as a large-scale rapid increase of Antarctic ice-volume (Alegret et al. 2008). It is a drastic change that started from the slow increase of ocean-temperature and decrease in continental ice-volume throughout the late Oligocene (Miller et al. 1991; Zachos et al. 2008; Beddow et al. 2015). The short period of climate warming during late Oligocene time is generally referred to as the Late Oligocene Warming Event (LOWE), or just LOW event, which was interrupted by several short glaciation events at the base of the Miocene, including the Mi-1 event, which occurred right at the Oligocene/Miocene boundary (Miller et al. 1991; Zachos et al. 1997). Recent results point to climatic perturbations mostly driven by changes in atmospheric CO_2 levels (O'Brien et al. 2020) from around 1000 ppm during the middle Eocene to less than 300 ppm at the Eocene–Oligocene transition (Foster et al. 2017). Such an intense and constant drop coupled with orbital variability is considered the trigger for Antartic glaciation. Sea surface temperature and biotic productivity clearly reacted to such global climatic perturbations (Torfstein and Steinberg 2020). During this event, several biotic turnovers took place in both planktonic and benthic communities (Alegret et al. 2008) and whilst in deep sea deposits these climatic perturbations are visible, the same punctual variations are hard to identify in shallow water settings. Shallow water ecosystems were most likely greatly affected by such climatic variations, but continuous stratigraphic sections in high hydrodynamic regimes are intrinsically characterized by chemical and physical factors that often hamper the clear recognition of such environmental perturbations. In fact, high hydrodynamics tend to rework fossil content (Seddighi et al. 2015; Briguglio et al. 2017), thus creating a mixture of autochthonous and allochthonous material, which can include contamination from much shallower deposits and so lead to a misinterpretation of the depositional setting. Occurrence and disappearance of taxa can be just local evidence due to the presence of competitors or due to a sudden unavailability of the ecological niche. Precise age indicators are also not as abundant as in the deep-sea record and even if present, their stratigraphic interval might not be accurate (Papazzoni et al. 2017). For all these reasons, the identification and calibration of such global climatic events is not always possible in shallow water deposits; nonetheless, dense sampling of extended stratigraphic sections might shed some light on faunal development during a period of climatic perturbation.

This work describes the stratigraphic development of a sedimentary sequence deposited during the late Oligocene along a section in NW Italy that displays a deepening trend from reefal shallow water conditions (Briguglio et al. 2021) into much deeper marine conditions, capped by turbidite deposits. Such conditions have the potential to preserve climatic variations within their fossiliferous content because the deepening trend contrasts with the prograding capacity of the hinterland, therefore reducing the sedimentary input to a minimum.

Geological setting

The stratigraphic section of Case Cné, here described and discussed, is located in the central sector of the Tertiary Piedmont Basin (TPB), close to the town of Dego (Savona Province), at the western edge of the Voltri Massif (Ligurian-Piedmontese oceanic domain, metaophiolites associated with metasediments; Capponi et al. 2016, and references therein), which is one of the tectonic units to form the Ligurian Alps.

The TPB is considered a late- to post-orogenic basin that, in the study area, unconformably overlies the tectonic pile of the Ligurian Alps (Gelati and Gnaccolini 1987; Mutti et al. 1995; Giglia et al. 1996; Capponi et al. 2001; 2009; Federico et al. 2015, and references therein), filled with non-marine to marine

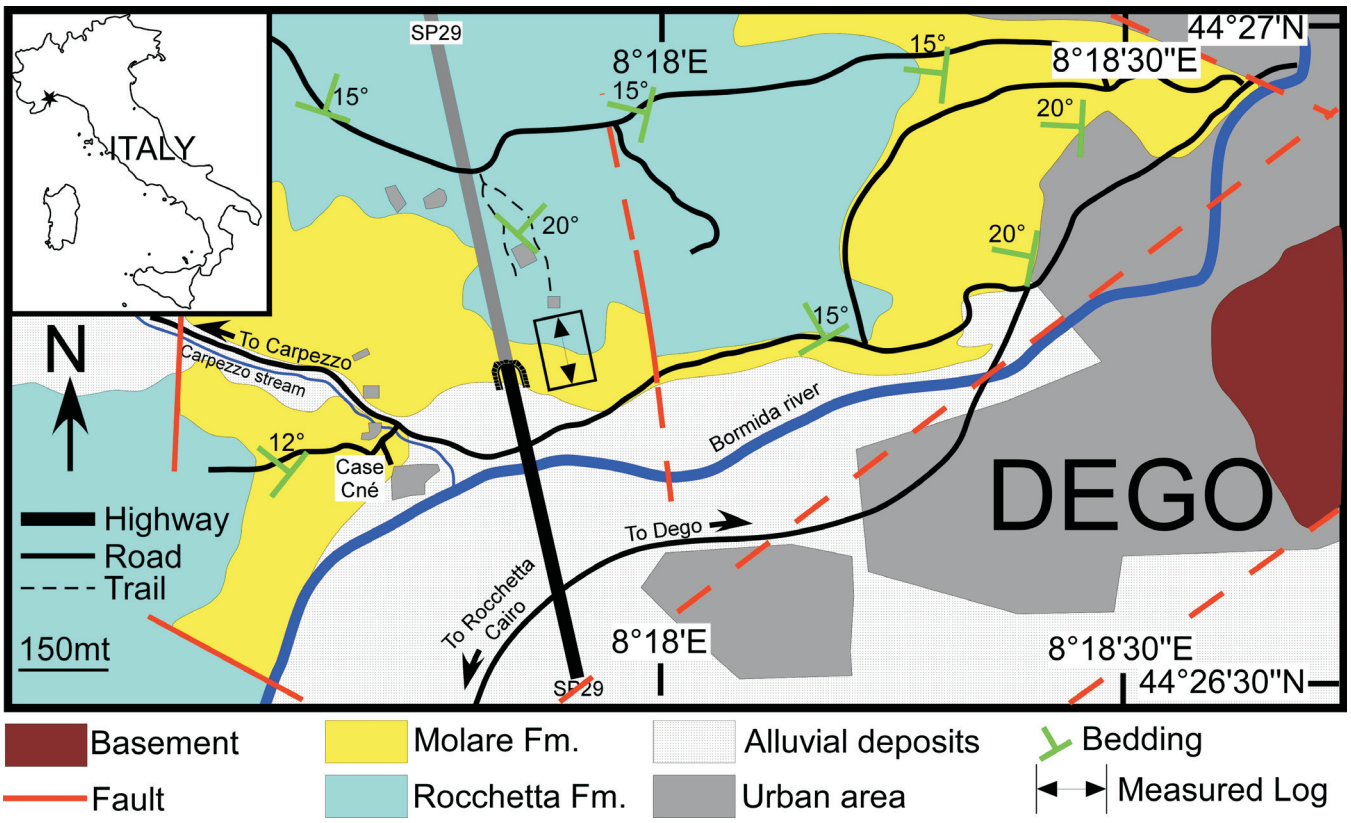

TEXT-FIGURE 1
Schematic drawing of the geology in the vicinity of Dego. The double arrowed line indicates the section.

sediments deposited from possibly late Eocene to the late Miocene. The Molare and Rocchetta-Monesiglio formations, that include a large part of the basal section of the TPB, were affected by the late-orogenic deformation of the Ligurian Alps, linked to the Corsica - Sardinia block rotation (Pasquarè 1968; Lorenz 1969; Capponi and Giammarino 1982; Gelati and Gnaccolini 1987; Bernini and Zecca 1990; Mutti et al. 1995; d'Atri et al. 1997; Capponi and Crispini 2002; Spagnolo et al. 2007; Quaranta et al. 2009; Gelati et al. 2010; Mosca et al. 2010; Bonci et al. 2011, 2018; Capponi et al. 2013; Federico et al. 2014, 2015, and references therein).

In the Dego area, serpentinites, metabasites and calcschists form the metamorphic substrate on which the sedimentary cover of the TPB was deposited. Sedimentation began with fine to very coarse nonmarine siliciclastic sediments, that were overlain by shallow marine sandstones and conglomerates and minor coral reef limestones, which pass to fine-to-medium sandstones followed by siltstones and marly siltstones; all these sedimentary units are grouped in the Molare Formation (Oligocene; Briguglio et al. 2021, and references therein). The Molare Formation records a transgressive rise in sea level that attained its acme with the deposition the Rocchetta-Monesiglio Formation (upper Oligocene - lower Miocene), which consists of silty sandstones, siltstones, and marls in which sandstone and conglomerate lenses are interbedded. For more detailed information about the geology and paleontology of the area of Dego the reader may refer to the aforementioned literature or to Ghibaudo et al. (2014a; 2014b) and Briguglio et al. (2021).

MATERIAL and METHODS

The studied section is situated in the locality Case Cné, in the vicinity of Dego (Province of Savona, Liguria, Italy), north of the small river Bormida di Spigno and east of the SP29 (provincial road 29). The base of the section is at the coordinates 44°26'43.82" N - 8°17'55.37" E and the top at 44°26'46.94" N - 8°17'53.11" E (text-fig. 1).

Age dating of the deposit was done by collecting well-preserved calcite shells of bivalves and measuring their strontium isotope content. Strontium isotope stratigraphy (SIS) is based on the fact that the Sr isotope ratio in the ocean varied through time and is homogeneous for any given time in the oceans and can be preserved in marine precipitate (e.g., McArthur et al. 2012). Therefore, the Sr isotopic ratio can be obtained from organisms that retained their original Sr isotope ratio precipitated from seawater and can be used for dating and correlation.

The Sr isotope curve of the last 590 Ma is kept consistently updated (McArthur & Howarth 2004; McArthur et al. 2012) and thus accurate chronostratigraphic dating may be achieved in time-intervals with especially steep trends in the Sr isotope curve. The transition from the Oligocene to Miocene is one of the periods where sedimentary rocks may be dated to a precision of 100 ky (Kocsis et al. 2018). The most accurate material

used for SIS is low-Mg calcite shells of bivalves (mostly pectinids and oysters) due to their high resistance to diagenetic alteration (McArthur 1994; Ullmann and Korte 2015). Throughout the section, three samples for strontium isotope analysis were taken at 13 m, 25 m and 30 m (text-fig. 2). The first two samples were extracted from oyster shells (*Pycnodonte brongniarti*) and the last sample was collected from a pectinid shell (*Pecten arcuatus*). These taxa were chosen because their original calcite biomineral has better preservation potential than aragonite shells (Trueman and Tuross 2002). The selected shells were checked for signs of recrystallization or crystal overgrowths, were cleaned in an ultrasonic bath to remove any adherent sediment and the external part was shaved off with a microdrill to avoid sampling any altered parts that may have come in contact with diagenetic fluid. The pectinid showed no signs of recrystallization whilst both oyster samples showed erosional structures and possibly poor preservation of the carbonate. Sr was separated using a standard cation exchange process, and then the isotopic ratios were analysed on a Finnigan MAT 262 thermal-ionization mass spectrometer. The long-term mean of modern seawater (USGS EN-1), measured at the laboratory at the time when the samples were analyzed was 0.709175 ± 0.000002 (2 s.e., n=436). The mean value of the USGS EN-1 standards run together with the samples analyzed for this study is 0.709197 ± 0.000005 (2 s.e., n=2). All the geochemical analyses were performed at the Institute for Geology, Mineralogy and Geophysics of the Ruhr-University (Bochum, Germany).

The $^{87}Sr/^{86}Sr$ ratios of the samples were corrected for interlaboratory bias, using the long-term Bochum value of this standard, to a value of 0.709175 for the USGS EN-1 standard to be consistent with the normalization used in the compilation of the ''look-up'' table of McArthur et al. (2001; version 4: 08/04). This table, which is tied to the Geological Time Scale of Gradstein et al. (2004) (GTS2004), was used to derive numerical ages from the studied samples. Minimum and maximum ages were obtained by combining the statistical uncertainty (2 s.e.) of the mean values of the Sr-isotope ratios of the samples with the uncertainty of the seawater curve. The numerical ages were then translated into chronostratigraphic ages and corresponding standard biozones by reference to the GTS2004.

For microfacies analysis, 118 thin sections were produced from the studied succession and were analyzed for their siliciclastic, biogenic carbonate components and interstitial fraction. Siliciclastic components have been evaluated based on their angularity (0 = very angular, 1 = angular, 2 = subangular, 3 = subrounded, 4 = rounded and 5 = well-rounded), grain size (1 = fine sand, 2 = medium sand, 3 = coarse sand and 4 = fine gravel) and dominant grain size (1 = coarse sand, 2 = medium sand, 3 = fine sand, 4 = silt and 5 = clay). The interstitial space was examined for presence/absence of elevated porosity (0 = absent, 1 = present) and for the material of the interstitial fraction (1 = clay, 2 = silt-clay, 3 = silt, 4 = clay and sparite and 5 = sparite) if present. The biogenic carbonate components were identified to a high taxonomic level (either to family level or higher), whilst larger foraminifera, whenever possible, were identified to the generic level (text-fig. 3a, Appendix 1). The occurrences of the fossil groups were semi-quantitatively ranked into rare = r, common = c and abundant = a. The results of the complete analysis are given in Table 1. Cluster analysis was performed using a UPGMA (= unweighted pair group method with arithmetic

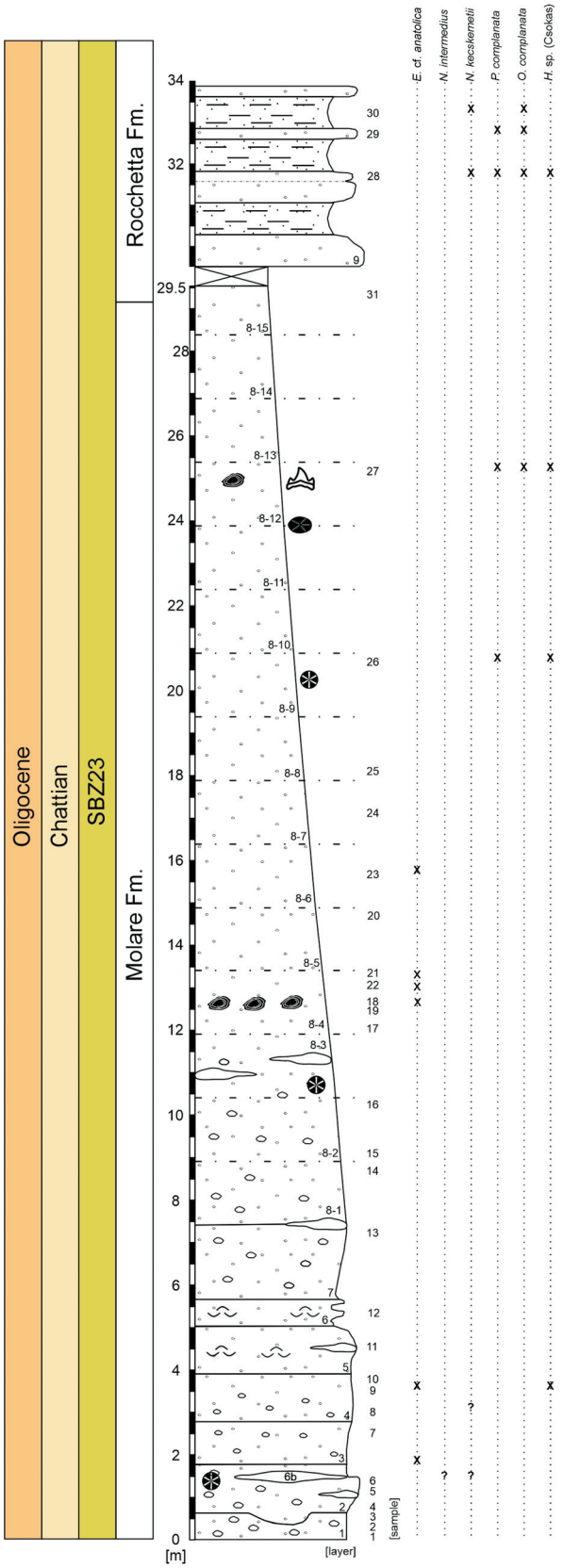

TEXT-FIGURE 2
Weathering profile of the studied section with indicated occurrence of larger foraminifera taxa based on oriented thin sections or identifiable section in the microslides.

TABLE 1
Abundance data of major bioclastic components from thin sections. A: abundant; C: common; R: rare.

	Acervulinid	Alveolinid	*Amphistegina*	*Astigerina*	larger Rotalid	*Nummulites*	*Operculina*	Lepidocyclinid	*Spiroclypeus*	*Planoperculina*	*Heterostegina*	*Sphaerogypsina*	*Victoriella*	SBF agglutinated	SBF hyaline	SBF porcellaneous	SBF fragment	planktonic foraminifera	Corallinacea	Halimedacea	Bivalve	Ostreid	Bryozoa	Coral	Echinoid	Gastropod	Serpulid	Ostracod	Decapod	Balanid
CNE1	-	-	R	-	R	R	-	C	-	-	-	-	-	-	R	R	-	-	A	-	-	R	C	-	R	-	R	-	-	-
CNE2	-	-	-	-	R	-	-	-	-	-	-	-	-	-	R	-	-	R	R	-	R	-	R	A	R	-	-	-	-	-
CNE3	-	-	R	R	R	-	R	C	-	-	-	-	-	-	-	R	R	-	A	-	R	R	C	-	R	-	R	-	-	R
CNE4	-	R	R	-	R	-	R	A	-	-	-	-	-	R	R	C	R	R	A	R	R	R	A	-	R	-	R	-	-	R
CNE5	-	R	C	R	C	-	R	C	-	-	-	-	-	R	-	R	-	-	A	-	R	-	C	R	R	-	R	-	-	-
CNE6	-	-	C	R	R	R	C	C	R	-	-	-	-	C	R	R	-	R	A	R	C	R	A	R	C	R	R	R	-	-
CNE7	R	-	C	C	R	R	R	C	-	-	-	-	-	R	R	R	-	-	A	R	R	R	A	-	C	-	R	-	-	-
CNE8	-	-	R	-	R	R	R	R	-	-	-	-	-	C	R	C	-	R	A	-	R	R	R	-	R	-	R	-	-	-
CNE9	-	R	-	R	C	-	R	R	-	-	-	-	-	C	R	C	-	-	A	-	R	-	C	R	A	-	R	-	-	-
CNE10	-	-	-	C	C	-	-	C	-	-	-	-	-	R	-	C	-	-	C	-	-	-	R	-	-	-	-	-	-	-
CNE11	-	-	C	C	R	R	R	-	-	-	-	-	-	R	-	C	-	-	A	-	-	-	C	-	R	-	R	-	-	-
CNE12	-	-	-	-	-	-	-	-	-	-	-	-	-	-	R	-	-	-	-	-	-	-	-	-	-	-	-	-	-	-
CNE13	-	-	R	-	-	R	-	-	-	-	-	-	-	-	-	-	-	-	R	-	-	-	-	-	-	-	-	-	-	-
CNE14	-	-	-	-	-	-	-	-	-	-	-	-	-	-	-	-	-	-	R	-	-	-	-	-	R	-	-	-	-	-
CNE15	-	-	-	-	-	-	-	-	-	-	-	-	-	-	-	-	-	-	R	-	-	-	-	-	-	-	-	-	-	-
CNE16	-	-	-	-	-	-	-	-	-	-	-	-	-	-	-	R	-	-	-	-	-	-	-	-	-	-	-	-	-	-
CNE17	-	R	C	C	-	R	R	R	-	-	-	-	-	R	-	R	-	-	R	-	R	-	R	-	R	-	-	-	-	-
CNE18	-	R	R	R	R	R	-	R	-	-	-	-	-	-	-	-	R	-	R	-	-	-	-	-	R	-	-	-	-	-
CNE19	-	-	C	R	-	-	R	C	-	-	-	-	-	-	-	-	-	-	C	-	R	-	C	-	-	-	-	-	-	-
CNE20	-	-	R	R	-	-	R	R	-	-	-	-	-	-	-	-	-	-	C	-	C	-	-	-	-	-	R	-	-	-
CNE22	-	-	C	R	R	R	C	A	-	R	R	R	-	-	-	R	-	-	R	-	-	-	C	-	R	-	-	-	-	-
CNE23	-	-	R	-	R	R	R	C	-	-	-	-	-	-	-	-	-	-	R	-	-	-	-	-	-	-	-	-	-	-
CNE26	-	-	C	-	-	-	A	R	-	R	-	-	-	-	C	C	-	-	R	-	R	-	C	-	C	-	-	-	R	-
CNE27	-	-	C	R	-	R	R	R	-	-	-	-	-	-	-	C	-	R	R	-	-	-	R	-	-	-	R	-	-	-
CNE28	-	-	C	C	-	-	A	R	-	-	R	-	R	-	-	-	-	R	-	-	-	-	C	-	R	-	-	-	R	-
CNE29	-	-	C	-	-	R	A	-	-	-	R	-	R	-	-	C	-	-	R	-	-	-	A	-	R	-	-	-	R	-
CNE30	-	-	-	-	-	-	R	-	-	-	-	-	-	-	-	-	-	-	-	-	-	-	R	-	-	-	R	-	-	-
CNE31	-	-	R	-	-	-	R	R	-	-	-	-	-	-	-	R	-	-	-	-	R	-	-	-	-	-	-	-	-	-

mean (with a Bray-Curtis Similarity Index) to check for specific groupings (text-fig. 4, Appendix 2).

Natural gamma ray spectra were measured along the section at approximately 30 cm intervals using the Codevintec Gamma Ray Surveyor Vario (VN6 Nal(Ti)) (text-fig. 3B). Based on these measurements, the abundance of Uranium (ppm), Thorium (ppm), Potassium (%) and gamma-ray (GR) dose rate (nGy/h) are inferred.

RESULTS

Description of the Case Cné section

The whole succession can be ascribed to a mixed siliciclastic carbonate sedimentation, with some layers that are sporadically devoid of carbonate components (text-fig. 2).

Layer 1 (~ 59 cm) consists of poorly sorted, siliciclastic and carbonate components and is a matrix supported pebbly conglomerate. The non-carbonate clasts are made up of serpentinite, metabasite, calcschist and quartz. The most abundant carbonate components are encrusting coralline algae. The contact with Layer 2 is diffuse and undulate.

Layer 2 (120 cm) is similar to Layer 1, however it contains more coral colonies (this is also visible in the microfacies (MF) slides) and is capped by a layer of encrusting coralline algae, creating a firm substrate for the overlying layer. Laterally, a lens with abundant larger foraminifera (LF) can be found; however, it is unclear if this part of the succession is *in situ* (sample 6b).

Layer 3 (100 cm) is composed of a fine conglomerate which fines upward and coralline algae dominate; some foraminifera of the genus *Nummulites* are present.

In Layer 4 (120 cm) the granulometry continues to become finer, but with slight lateral variations; at the base no fossils are clearly visible, but near the top large foraminifera occur together with some bioturbation (domichnia).

Layer 5 (108 cm) shows a change from a fine conglomerate of the lower layers to a sandier lithology; in some layers there are visible bivalve shells. The grain size is between fine and medium sand with better sorting than before; a more competent sandier lens is visible within this layer.

Layer 6 (69 cm) consists of strongly alternating lithologies. It starts with a silty-clay sublayer with intercalated sandstone laminae, followed by a bed of sandstone, then a silt-clay horizon and capped by a sandstone bed. The overall granulometry is medium sand and layers of bivalve shells are visible.

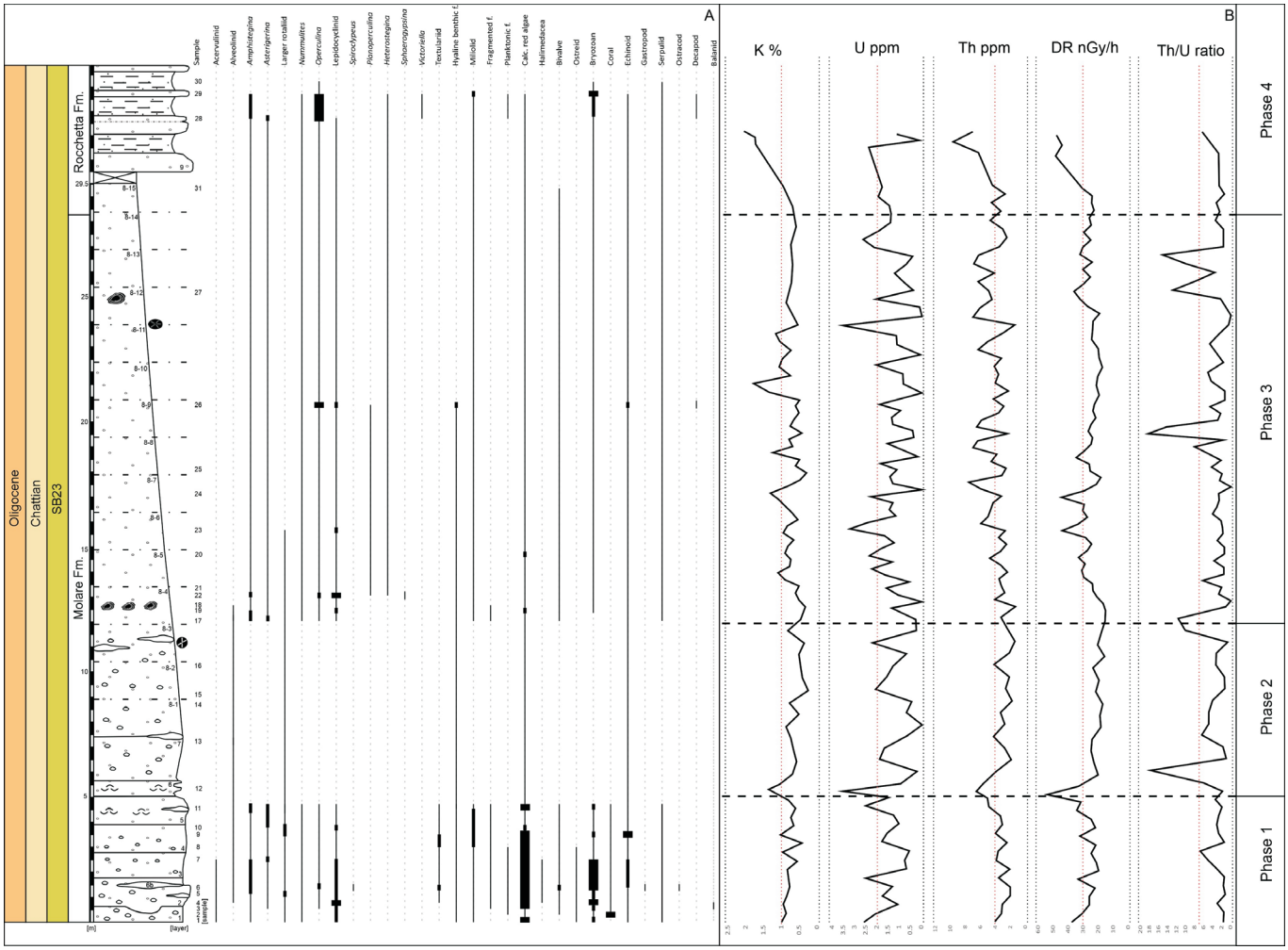

TEXT-FIGURE 3
Distribution of taxa and gamma ray spectra. A) Schematic drawing of the studied sections with key occurrence of important fossil groups; B) results of the natural gamma ray survey.

Layer 7 (178 cm) records a drastic change in lithology, as it shows again the same fine conglomerate as seen in the lowest layers.

From Layer 8 (22.5 m) to the base of layer 9 (29.5 m), the succession is composed of laterally strongly discontinuous, wavy, non-parallel beds with variable thickness and lateral extension. The individual beds cannot be separated and therefore this part is treated collectively. Throughout this section, the siliciclastic components are made up of serpentinoschists, metabasites, calcschists and quartz of coarser grain sizes in the lower part and finer grain size towards the upper part of the layer, where abundant bioclasts also appear. This part of the succession crops out nicely until it disappears due to field/meadow overgrowth. It can only be speculated that these gaps represent the finest part of the succession which was then weathered.

The final part of the studied section can be found approximately 65 m NNE from the top of Layer 8 and the contact between these two layers remains unclear. It consists of 440 cm of alternating pelitic sediments, containing irregular echinoids and coarser beds with abundant larger foraminifera. Locally abundant shells of pectinids can be found. Unfortunately, this part of the section was last exposed and accessible in June 2019, as part of a construction site, which is now covered.

Microfacies Analysis

Based on an UPGMA the thin sections of the complete profile were summed into four major microfacies (MF) clusters (text-fig. 4). The semi-quantitative abundance of fossil content throughout the section is reported in text-figure 3A. Microfacies 1 (MF1) can be recognized in samples CNE1 to 11, with exclusion of CNE2, as all the thin sections obtained include large coral fragments. This MF is defined by a high amount and diversity of carbonate components. The most abundant components are fragments of coralline algae, followed by bryozoans and lepidocyclinids, followed by common occurrence of porcelaneous smaller benthic foraminifera (SBF), echinoid fragments and *Amphistegina, Asterigerina* and other unidentifiable larger rotaliids. There are also rare fragments of corals, bivalves (including oysters), gastropods and serpulids, together with rare acervulinids, alveolinids,

Nummulites, Operculina, Spiroclypeus (?), hyaline and agglutinated SBF, planktonic foraminifera, and halimedacean algae. The siliciclastic components are also diverse in these layers and the common characteristics of this MF are based on the diversity of the biogenic components. Angularity of clasts range from angular to rounded; the largest clasts of this MF type range mostly between medium and coarse sand and in only some cases fine sand or fine gravel. Overall, siliciclastic components range mostly between coarse and medium sand; in CNE9 and 10, fine sand is dominant. The interstitial space is filled mostly by sparite and clay and porosity is low. In Microfacies 2 (MF2), found in CNE12 to 16 and CNE31, the siliciclastic components are dominant and some samples can be considered nearly barren of fossils. There are rare occurrences of echinoid fragments, *Amphistegina, Nummulites*, small hyaline and miliolid foraminifera and fragments of coralline algae. The angularity of the siliciclastic components ranges from angular to subrounded, with rounded grains in some samples (CNE15 and 16). The largest clasts are mostly fine gravel or very coarse sand and the interstitial component locally consists of sparite with rare clay pockets in some samples. The dominant clastic fraction ranges from fine to coarse sand. Sections from samples CNE 13 to 15 show a remarkably high porosity.

Microfacies 3 (MF3) is variable and includes samples from CNE17 up to CNE27 except for CNE26. These samples are generally richer in biogenic carbonate content, but due to the strong variability within the larger foraminifera associations and consistency of the siliciclastic components they have been further subdivided into three submicrofacies.

MF3.1 (CNE17, 19, 22), characterized by the common occurrence of bryozoans, *Amphistegina*, and lepidocyclinids and rare occurrences of bivalve and echinoid fragments, alveolinids, *Asterigerina, Nummulites, Operculina, Planoperculina, Heterostegina, Sphaerogypsina*, larger rotaliids, small miliolids, agglutinated foraminifera and coralline algae fragments. The siliciclastic components are angular to well-rounded; the largest clast is fine gravel and the interstitial component consists of clay and sparite. The dominant fraction of clastic components is between medium to fine sand.

MF3.2 shows no dominance of a single fossil group, but has rare occurrence of bryozoans, bivalve fragments, serpulids, *Amphistegina, Asterigerina, Nummulites, Operculina,* lepidocyclinids, larger rotaliids, miliolids, and coralline algae fragments. The siliciclastic components are more diverse in this submicrofacies with angularity from angular to subrounded; the largest clasts are coarse sand with a clayey/sparitic interstitial component. The dominant fraction of clastic components is fine sand.

MF3.3 is only present in CNE18 and is defined by a change in the clastic components rather than in the biogenic ones. The angularity of the clasts is between angular and subrounded, the matrix is silty, and the dominant fraction is medium sand. However, the largest clasts reach up to fine gravel; this sample has a high porosity.

Microfacies 4 (MF4) is different from other microfacies in that it has a high abundance of larger foraminifera and a clay matrix (samples CNE26, 28, 29 and 30). It is a larger foraminifera packstone, with the exception of CNE30, which has a higher abundance of matrix. The most abundant carbonate component is *Operculina*, but there are common occurrences of bryozoans, *Amphistegina* and miliolids. Additionally, there are rare occurrences of bivalve and echinoid fragments, decapods rests, serpulids, *Asterigerina, Nummulites*, lepidocyclinids, *Planoperculina, Heterostegina*, *Victoriella* and hyaline SBF. The siliciclastic components are between angular to rounded and the largest clasts are between fine and coarse sand; the interstitial component is between clay and clay/sparite.

Gamma Ray

The most common K-bearing minerals in sedimentary rocks are K-feldspar, mica and illite. While K-feldspar and mica are more common in sandstone, illites are typically found in shales. Potassium can only be regarded as a good indicator for clay content in the absence of significant amounts of K-feldspar grains or smectites of poor K content (Fabricius et al. 2013). Throughout the section, the %K curve (Fig 3B) fluctuates between 0.5 and 1.5%, exceeding these values only once at 21.5 m. From 25 m the K content remains constant until Layer 9, where it begins to increase continuously.

The Th/U ratio is regarded as a good proxy for sedimentary processes; it ranges in this section from 0.02 to more than 21, where values below 7 are regarded as indicative of deposition in a marine environment (Adams and Weaver 1958). Values below 3.0 are interpreted to indicate abundant authigenic U under anoxic conditions (Wignall and Myers 1988), Chen et al. (2016) regard the U content and Th/U ratio as good proxies for total organic carbon (TOC) and in general for oxidative versus reductive palaeoenvironments. They report that if TOC is higher than 4%, organic matter controls the enrichment of U under calm and reductive conditions. However, very low Th/U ratios should be regarded with caution since carbonate content may influence Th and U content massively (Adams and Weaver, 1958). Nevertheless, in stable marine environments with high carbonate content, GR curves and TOC most likely reflect U enrichment due to change in hydrodynamic regimes, rather than productivity and terrigenous input (Ehrenberg et al. 2008, Reuter et al. 2013).

According to the data here obtained (text-fig. 3b), the Th/U ratio remains mostly within the margin of marine sediments. However, it shows some distinctive peaks that exceed the upper limit of marine sediments at 6 m, 12 m, 20 m and 25.5 m, which always coincide with a change in microfacies. Specifically, there are three distinct negative shifts in the Th/U ratio at 13 m, 24 m and 25 m, that co-occur with an increase in U and a decrease in Th, and with an occurrence of large oyster shells visible on the profile. The Th and U curves can generally be separated into three parts (text-fig. 4B). The lower part is from the base of the section up to 12 m and shows low frequent fluctuations. The middle part has frequent fluctuations and the upper part is more stable towards the pelitic upper part of the succession. The middle part of the succession exactly coincides with MF3.

Biostratigraphic remarks and geochronological dating

The chronostratigraphic assessment of the section was attempted by using the occurrence of larger foraminifera throughout the section. It is based on the biozonation scheme by Cahuzac and Poignant (1997) with additional implementations by Özcan et al. (2009, 2010), Less et al. (2018) and Parente and Less (2019). Identification is based on orientated thin section from isolated specimens or sections within the microfacies slides (text-figsd. 5 and 6). Especially in the lower part of the succession, the LF assemblage is dominated by lepidocyclinids

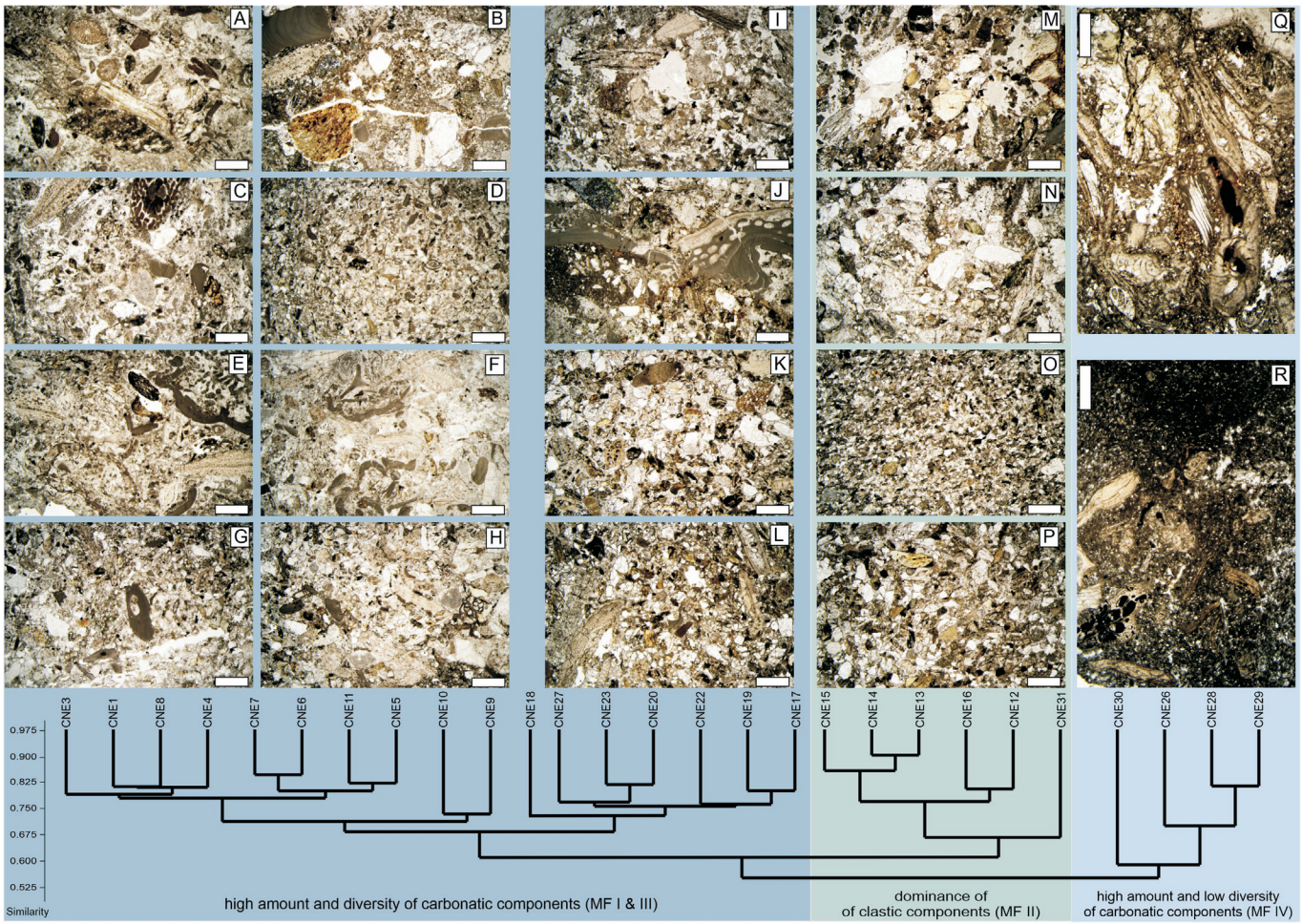

TEXT-FIGURE 4
Principal separation of the encountered microfacies types in the Cné Section.
Representative microslides are plotted versus the dendrogram of the UPGMA

(A) CNE1 ; (B) CNE3; (C) CNE4; (D) CNE8; (E) CNE6; (F) CNE7; (G) CNE9 ; (H) CNE11; (I) CNE18; (J) CNE20; (K) CNE22; (L) CNE23; (M) CNE14; (N) CNE31; (O) CNE12; (P) CNE16; (Q) CNE28; (R) CNE30.

which are here tentatively identified as *Eulepidina* cf. *anatolica*. This uncertainty is mainly due to the fact that correct identification is usually based on biometric parameters retrieved on large-size populations of at least 10 to 15 individuals. Here only three specimens could be analysed biometrically and their values (measured according the mentioned literature) do not permit conclusive determinations. The specimen in text-figure 6D is characterized by the following measurements: D: 515 µm, P: 281 µm, A: 60, n:14 and consequently should belong to the genus *Eulepidina* rather than *Nephrolepidina* by the high A value and could be identified more specifically to *E. anatolica* but with a rather small proloculus diameter that has never been reported of this size. The specimen figured in 6E has the biometric parameters as follows D: 664 µm, P: 366 µm, A: 82, n:14 and could be again an *Eulepidina* cf. *anatolica* characterized by an unusually small embryo that should classically be P < 400 and D < 650. The specimen figured in 6F has the following values: D: 630 µm, P: 377 µm, A: 65, n:14 and again cannot be considered as a member of the genus *Nephrolepidina* but as an *Eulepidina anatolica* with a smaller embryo than the published values for the same species. *Eulepidina anatolica* is typical in the upper Chattian (Less et al. 2018, Parente and Less 2019).

The nummulitid foraminifera *Operculina* and *Nummulites* are present from the lowest parts of the sections, but no specimens could be isolated and thus *Nummulites* sp. and *N. kecskemetii* could only be identified from random oblique and axial sections (text-figs. 5 A-B,6 A-C). The upper part of the section (above CNE22) shows a decrease in abundance of lepidocyclinids and a general increase in abundance of *Operculina complanata*

(text-fig. 5E) and later within the section the first appearance of *Planoperculina complanata* (CNE22; text-fig. 5C). Only few specimens could be isolated up to sample CNE26; the higher clay content within MF IV allowed for better maceration of samples from CNE26 upward. *Heterostegina* sp. (Csokas) (text-fig. 5D) is present in the lowermost part of the section (CNE9) and is documented by oriented section at least up to CNE26.

The nummulitid species here identified, i.e., *Planoperculina complanata, Heterostegina* sp. (Csókás), *Nummulites kecskemetii*, *Operculina complanata* and *Eulepidina anatolica* are characteristic of the NE Hungarian late Chattian SBZ 23 Zone (Less, 1991).

However, due to the lack of isolated specimens or equatorial sections in the MF slides, it is unclear if the lower part of the section should be assigned to SB23 or 22B. Nonetheless, the reefal complex outcropping below this measured section has convincing evidence suggesting an age comparable to this material.

In the reefal sediments, *Nephrolepidina* cf. *morgani* and *Eulepidina anatolica* were recorded, thus indicating placement in SB23. For this reason, the entire section here presented is regarded as SB23.

Strangely, there is a complete lack of *Miogypsina* throughout the whole section, which should already be present in SB23 (Parente et al. 2018). The overall change in dominance from lepidocyclinids to nummulitids in the section can interpreted as a palaeocological rather than a biostratigraphic signal, since all lepidocyclinid taxa recognized from this section would reach the lowermost Miocene and thus into the Rocchetta-Monesiglio Formation at the top of the studied section (text-fig. 2B).

The results obtained from Sr isotope dating indicate an age interval that seems to validate the LBF chronostratigraphic assessment. Unfortunately, the oyster collected in the lower part of the profile, with poorly preserved material gave relatively younger age results (min: 18.06 Ma; mean: 18.20 Ma; max: 18.34 Ma). The other two samples collected appeared to be more pristine in structure and composition. The oyster collected at 24 m gave the following ages: min: 26.89 Ma; mean: 27.34 Ma; max: 27.76 Ma; and the pectinid collected near the end of the section indicates ages as following: min: 23.92 Ma; mean: 24.20 Ma; max: 24.49 Ma.

The LOW is an event that peaked at 24 Ma and therefore is possibly represented by the upper part of the measured profile.

DISCUSSION

Depositional development

Based on the litho-, bio- chemostratigraphic, and microfacies analyses, the timing and depositional development of the Cné section was reconstructed. According to Briguglio et al. (2021), whose study is focused on the reefal outcrops just below the sedimentary sequence here presented, the general depositional environment is characterized, during its early stages, by a fluvial system that delivered siliciclastic material into this sector of the Tertiary Piedmont Basin from the south to the north (modern), cutting through local topography with steep relief. The entire depositional succession includes a sequence of terrestrial landslides, submarine talus deposits, marginal marine conglomerates, a reefal complex and the subsequent capping of the reef. The present work starts at the suffocation phase of the reef complex by fluvial activity and the following drowning by a transgressive event. According to the obtained data, we identified four different phases.

Phase 1 documents the suffocation of the underlying reef, which includes the first five layers of the Cné Section (up to sample CNE11) where an abundance of biogenic carbonate components is intermingled with rather coarse siliciclastic components. In Dèchet (1996) this lithofacies is described as fossiliferous fine conglomerates and can be ascribed to the movement of the main transport trajectory of the fluvial system onto the reef. This mixture of lithology is especially evident in the lowermost parts (layers 1-3) where the dominant clasts size consists of coarse sands and large coral fragments (CNE2). Towards the top of Layer 5 the grain size becomes finer (medium-fine sands), while the interstitial component throughout the whole part of this section is made up dominantly of sparite with local clay pockets. This may indicate higher water energy, but not high enough to completely remove the clay fraction. The strong mixture of different angularities may also be attributed to the different mineralogy of the clastic components than as an indication of different transport distance. Likewise, the high diversity and size differences of biogenic carbonates in these layers may indicate a rather short transport for the carbonate components. However, it is unclear if carbonate components in this phase are sedimented together with the clastic components or if the high diversity of biogenic carbonate is solely due to reworking of the reef complex by fluvial transport (text-fig. 4A).

Phase 2 is characterized by stronger activity of the fluvial system and a much higher input of clastic sediments, as documented by MF2, which is nearly barren with only rare occurrence of some fossil groups. The phase initiates with a package of alternating pelitic sediments and fine sandstones (Layer 6) which indicates an extremely rapid change of the hydrodynamic regime. Up section until the lower part of layer 8, there is a reoccurrence of the fine conglomerate lithology. Specifically, samples CNE13, 14 and 15 are distinct since they all consist dominantly of fine gravel with sparry cementation and high porosity, overlain by Layer 8-3 (sample CNE16) which has low porosity and local clay pockets and is finer (coarse sand) than the previous layers. Directly above this sample, lenses of finer sediment and sporadic corals occur together. The pelitic layers and the fine lenses throughout Layer 6 reflect local and short term changes in the mode of deposition and may indicate more distal fluvial deposits with strong lateral variations. However, the overall change to coarse sediments and abundant sparry cementation of Layer 8 (sublayer 1-3) might indicate a prograding phase of the fluvial system due to a short-term pause in the transgressive process (possibly due to local tectonics). The first two phases of the succession point to a more fluvial influenced setting rather than an overall transgressive trend. The fining upward trend observed in phase 1 might be interpreted as a deepening sequence and the coarsening upwards trend in phase 2 to progradation. The shift in the mode of sedimentation is also reflected in the natural gamma ray spectra, especially in the change in abundance of U and Th, which oscillate with a much lower frequency from Layer 1 to Layer 8-3 and with a much higher frequency in the rest of the section.

Furthermore, at the onset of the short coarsening upwards trend, a peak in the Th/U ratio can be observed (text-fig. 4B). These

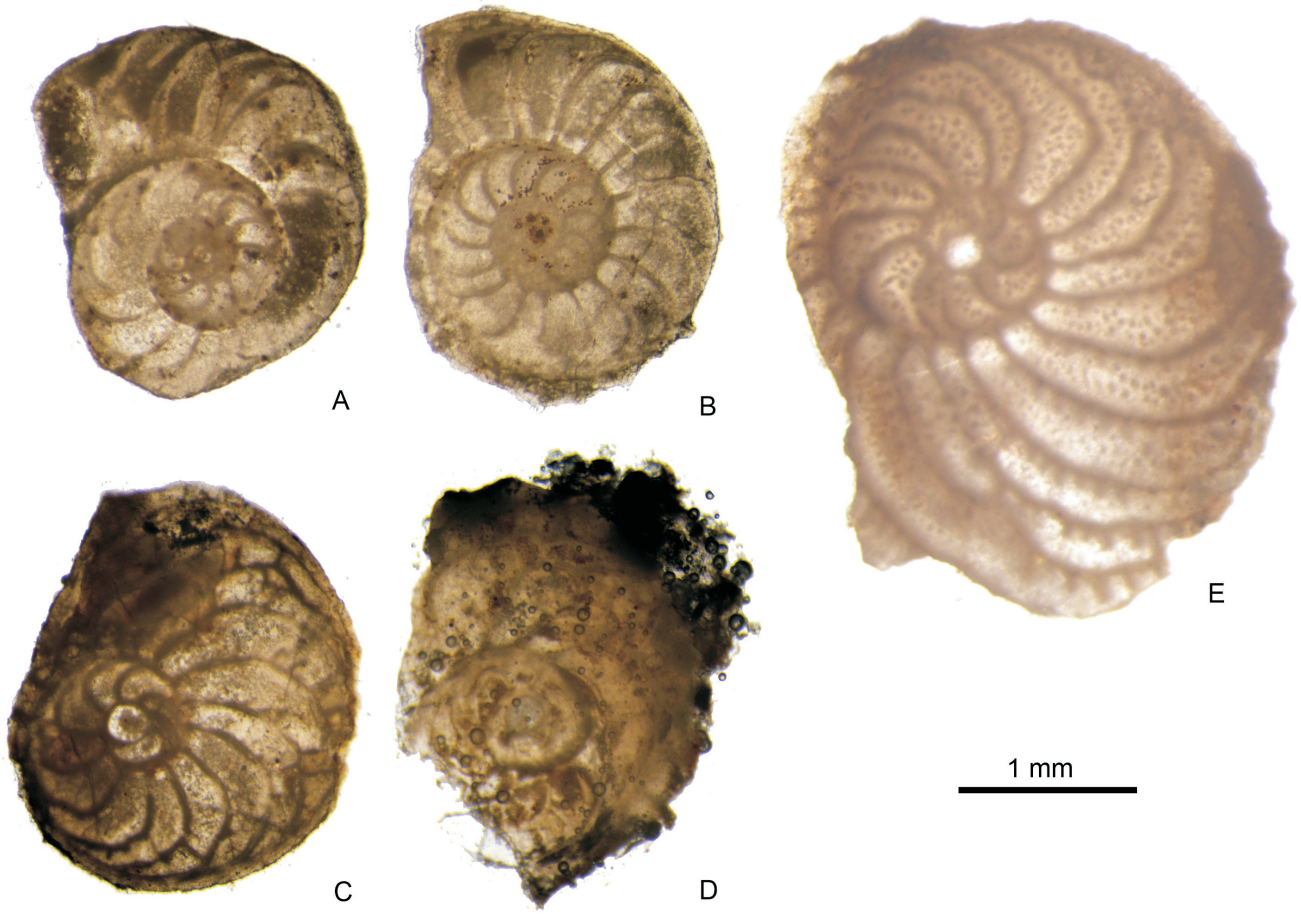

TEXT-FIGURE 5
Equatorial sections of representative specimens of the larger foraminifera assemblage (1).

A-B *Nummulites kecskemetii* (A CNE26-3; B CNE30-2)
C *Planoperculina complanata* CNE27-9
D *Heterostegina* sp. (Csokas) CNE9-2
E *Operculina complanata* CNE27-2

variations could be linked to the change from a transgressive system tract to a short lived high-stand system tract where deposition is greater than accommodation space, resulting in progradation. Indeed, based on the chronostratigraphic assessment of the middle to the upper part of the section, an incipient warming period most likely resulted in increased weathering, which resulted in a greater supply in coarser sediments to the system. The peculiar size of the lepidocyclinids retrieved in this succession, which are characterized by a smaller proloculus and deuteroloculus sizes, can be linked to a depositional environment that did not fulfil the ecological requirements for those taxa. Similar variations have been observed since the pioneering studies by Pecheux (1995) and further confirmed by numerous studies in both modern (Eder et al. 2016, 2017, 2018) and fossil settings (Torres-Silva et al. 2017). Whether the lepidocyclinids here retrieved represent a newly undescribed species cannot be ruled out and requires further study.

Phase 3 is the longest and most diverse depositional phase within the Cné section. It documents the final drowning of the shallow marine reefal complex during the transgressive phase. A second maximum in Th/U ratio, just above the last occurrence of corals in the section, at sample CNE17, is recorded at its base. The transition from phases 2 to 3 is documented by a change from MF2 to MF3, which is more carbonate dominated but much less diverse than MF1. Within the carbonate components, the dominance shifts from coralline algae and bryozoans to a more diverse larger foraminifera assemblage, whereas in the clastic components a clear fining upwards trend can be seen. The larger foraminifera assemblage changes from dominant lepidocyclinids to

nummulitids (*Operculina complanata*, *Planoperculina complanata*, *Heterostegina* sp., *Nummulites kecskemetii*). CNE17 is followed by a bed of *Pycnodonte brongniarti*, which co-occurs with a minimum in the Th/U ratio and a subsequent trend in increasing U abundance (text-fig. 3B). This increase is continuous throughout most of MF3 and could be a consequence of a continuous warming trend during this portion of the late Oligocene. Additionally, the benthic community changes from lepidocyclinid dominated to nummulitid dominated. The third peak in the Th/U ratio can be found just below sample CNE26, which is a locally and stratigraphically limited occurrence of MF4 with an abundance of operculinid LF, bryozoans and fine-grained matrix. Just below sample CNE27, complete irregular scutellid echinoids and large *Pycnodonte brongniarti* co-occur associated with a peak in U and a low in the Th/U ratio. The final Th/U maxima (double peaks), as well as the oscillation in the U, Th and K may indicate a final change in the depositional environment; at this point, sediments become finer and more pelitic and document the transition from the Molare Formation into the Rocchetta-Monesiglio Formation, which is deposited in a completely different setting. Sample CNE31 can be attributed to MF2, and has coarse clastic components with minor biogenic carbonate; the matrix consists of silt to clay, and is consistent with the fining upwards trend of the upper part of the section. In summary, phase 3 documents the change from a strongly fluvialaly-influenced setting to a depositional system that is mostly characterized by event gravity flows. High frequency oscillations in the Th and U curves in this part of the section indicate an unstable sedimentary regime, typical of prodelta deposition where even reductive and oxidative environments can alternate. Alternately, the interpretation by Chen et al. (2016) that high values in U might reflect higher values of TOC could also apply. This argument is strengthened by the presence of the *Pycnodonte* beds at the onset of the increasing U trend, which would thrive as a filter feeder in environments with abundant TOC. The same can be interpreted for the cooccurrence of high U abundance at the layers with the irregular echinoids and *Pycnodonte* below sample CNE27.

Contrary to MF1, the biogenic carbonates from MF3 cannot derive from the reworking of the underlying reef complex and thus must be regarded as transported into the depositional environment from the more protected shallow-marine areas adjacent to the river mouth. This is further exemplified by the change of the LF assemblage from lepidocyclinids to nummulitids (especially, *Heterostegina*, *Planoperculina* and *Operculina*), since these latter are known to adapt more readily to environments of higher light attenuation, for instance through high terrigenous input near fluvial systems, by back-stepping or morphological adaptation (Eder et al. 2018; Goeting et al. 2018). A warming climate might be responsible for this change in sedimentary regime affecting both substrate composition and irradiation depth by reducing water transparency, thus producing such a shift in the benthic community.

Th/U ratios exceeding 7 are classically interpreted as evidence for terrestrial environments (Adams and Weaver 1958); those documented throughout the section in phase 2 and 3 are quite enigmatic in this sedimentary context but might also indicate that these deposits originated well into the onshore and were transported by riverine activities to the shallow marine setting during storms. The fact that they are connected to a major change in the depositional development indicates that these ratios are not due to measurement errors. Furthermore, they do not correlate with a high abundance of Th but rather with a low abundance of U, which would indicate well-oxygenated environments.

Phase 4 is the last and the final phase of the depositional environment of the described section and documents the "turbiditic" deposits of the Rocchetta-Monesiglio Formation. The transition between the two formations generally doesn't crop out very well throughout the TPB, since the uppermost part of the Molare Formation becomes consistently more pelitic and is easily eroded, which is also the case in the Cné section (Gelati et al. 2010, and references therein). The sediments of the Rocchetta-Monesiglio Formation developed as an alternating succession of silty beds with abundant larger foraminifera and more pelitic beds with irregular echinoids and sporadic occurrence of larger foraminifera, both grouped together in MF4. The sedimentation of this phase documents the full development of the transgression and biogenic components and were mostly transported by turbidity flows into the pelagic realm. This is further indicated by the overall similarity of shape and size of the larger foraminifera assemblage of MF4, which is common in geological sections documenting the redeposition of larger foraminifera into deeper-marine settings (Torres et al. 2019).

CONCLUSIONS

Utilizing information collected on the litho-, bio- and chemostratigraphy, the depositional evolution, timing and its influencing factors for the Cné Section is reconstructed. The studied succession of mixed siliciclastics and carbonate deposits was deposited into the Tertiary Piedmont Basin during the late Oligocene (SBZ23) by an active small-scale fluvial system to the east (modern) and an active small-scale carbonate factory, in a more-protected position due to the local topography, to the west (modern). It documents the suffocation of the underlying local fringing reef complex by the nearby fluvial system and the successive drowning of the carbonate producers by a shift towards a transgressive system during a period of increasing warmth. Furthermore, it documents the transition of the Molare Formation, dominated in the lowermost part by mixed sediments of fluvial sediments and reworked carbonates followed by a continuous fining upwards trend, into the lower part of the Rocchetta-Monesiglio Formation, which developed as a sequence of turbidity flows. The overall depositional development of the succession can be summed up in four phases. The first phase documents the suffocation and reworking of the underlying complex by the fluvial system documented by an overall fining upwards sequence with high diversity and abundance of carbonate components. During phase 2, the depositional environment was strongly influenced by the fluvial system and was dominated by siliciclastic components. This is especially indicated by the initial coarsening upwards trend which later changes to a fining upward trend of the sediments. It is, however, unclear if this can be explained only by lateral movement, since the river was strongly restricted due to the surrounding metamorphic lithologies. The end of this phase is characterized by a resumption of carbonate production and lower hydrodynamic energy is indicated by the presence of fine sediment lenses and corals. Phase 3 documents the final change of the fluvial system, hampered by transgression, and an overall fining upwards in the clastic components. Carbonate components are less diverse than in phase 1 but are dominated throughout by larger foraminifera. The change of the LF assemblage towards flat nummulitids (*Planoperculina, Operculina* and *Hetero-*

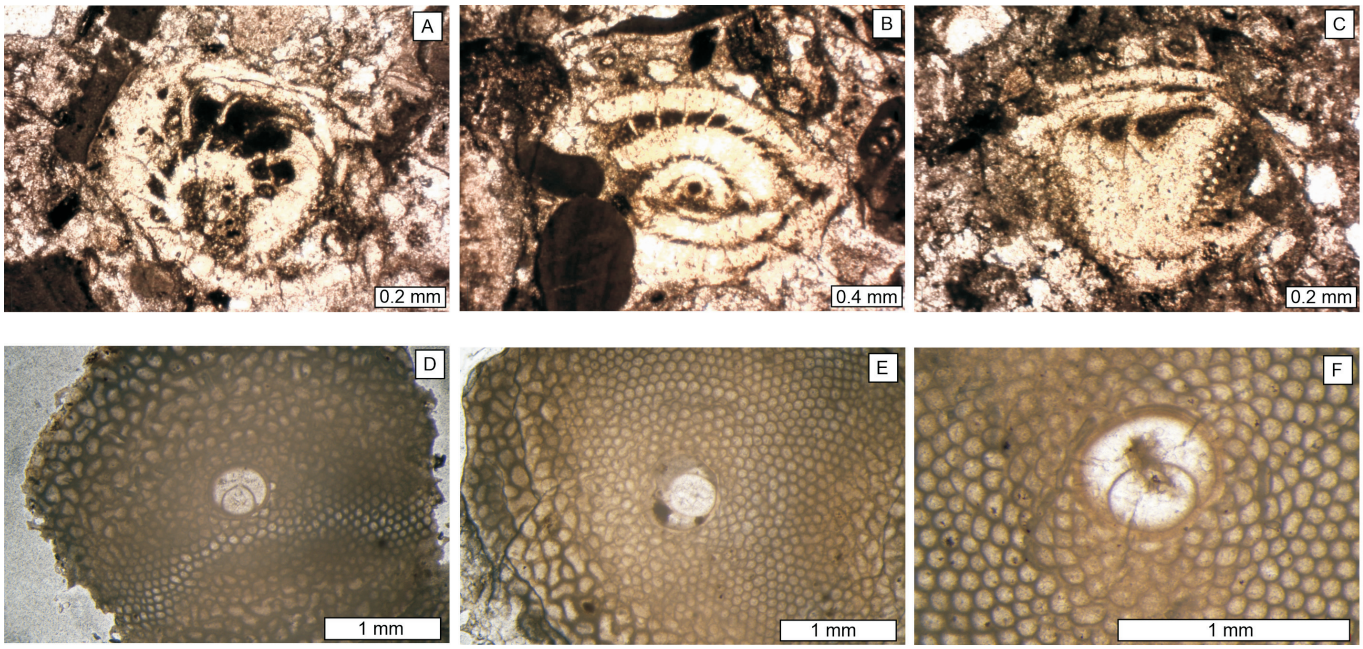

TEXT-FIGURE 6
Representative specimens of the larger foraminifera assemblage (2).

A Oblique section of *Nummulites kecskemetii* CNE6-1;

B-C oblique sections *Nummulites* sp. (A CNE6-3; B CNE8-1);

D equatorial section *Eulepdina* cf. *anatolica* CNET2-1;

E equatorial section *Eulepidina* cf. *anatolica* CNE221;

F equatorial section *Eulepdina* cf. *anatolica* (CNET2-1).

stegina) may indicate a reduction of the photic zone due to higher light attenuation, which is also supported by the presence of *Pycnodonte brongniarti* beds and irregular echinoids correlating with high abundance of U. All of these changes suggest transition to a warming climate that resulted in increased precipitation, enhanced erosion, and sediment transport. Sedimentation during this phase was gravity flow event beds, which show a laterally changing thickness and lithology. The last phase documents a gradual change to more pelagic sediments and finally passes into the turbiditic sequences of the Rocchetta-Monesiglio Formation. This part of the sedimentary succession alternates between pelitic layers with fewer lager foraminifera and irregular echinoids and "coarser" (silty clay) beds dominated by operculinid larger foraminifera and bryozoans, possibly as allochthonous material from the more proximal settings.

The natural gamma-ray spectra were a valuable tool used to distinguish the different phases of the depositional development. Especially, the frequency in oscillations of the U and Th curves clearly distinguish sedimentation influenced by the fluvial system, gravity flows and the full on-set of the transgression.

Furthermore, enigmatic peaks within the Th/U ratio are extremely interesting since they are not driven by high Th values but rather low U values, which may indicate short-term phases of high hydrodynamic energy (e.g., storm-events).

ACKNOWLEDGMENTS

We thank undergraduate student Clarissa Bruzzone for her help in the field, Wolfgang Eder (ex-University of Genova) for his contribution to this work and S. Riechelmann and A. Immenhauser (both Ruhr-University Bochum, Germany) for Sr isotope analysis. This work has greatly been improved by the comments of George Less, Gianluca Frija and the editor Jean M. Self-Trail. This study was made possible through the financial support by the University of Genova under the Curiosity-Driven projects - 1000222018-AB-CURIOSITY_001 and got substantial contribution by PRIN project 2017RX9XXY_002.

REFERENCES

ADAMS, J.A.S. and WEAVER, C.E., 1958. Thorium to uranium ratios as indications of sedimentary processes: Example of concept of geochemical facies. *American Association of Petroleum Geologists Bulletin,* 42: 387–430.

ALEGRET, L., CRUZ, L. E., FENERO, R., MOLINA, E., ORTIZ, S. and THOMAS, E., 2008. Effects of the Oligocene climatic events on the foraminiferal record from Fuente Caldera section (Spain, western Tethys). *Palaeogeography, Palaeoclimatology, Palaeoecology,* 269: 94-102.

BEDDOW, H. M., LIEBRAND, D., SLUIJS, A., WADE, B. S. and LOURENS, L. J., 2015. Global change across the Oligocene-Miocene transition: High-resolution stable isotope records from IODP Site

U1334 (equatorial Pacific Ocean). *Paleoceanography and Paleoclimatology,* 31: 81–97.

BERNINI, M. and ZECCA, M., 1990. Le deformazioni nella Formazione di Molare e Rocchetta (Oligocene e Miocene inferiore) della regione di Mioglia (SV) (Margine sud del Bacino Terziario Piemontese). *Atti Ticinensi di Scienze della Terra,* 33: 1–10.

BONCI, M.C., DABOVE, G.M. and PIAZZA, M., 2018. The Oligocene mollusc types of Gaetano Rovereto from Santa Giustina and Sassello (NW Italy). *Carnets de Géologie,* 18: 281–303.

BONCI, M.C., VANNUCCI, G., TACCHINO, S. and PIAZZA, M., 2011. Oligocene fossil leaves of the Perrando collection: history, preservation, and paleoclimatic meaning. *Bollettino della Società Paleontologica Italiana,* 50: 145–164.

BRIGUGLIO, A., SEDDIGHI, A., PAPAZZONI, C. A. and HOHENEGGER, J., 2017. Shear versus settling velocity of recent and fossil larger foraminifera: New insights on nummulite banks. *Palaios,* 32: 312–329.

BRIGUGLIO, A., VANNUCCI, G., BRUZZONE, C. and PIAZZA, M., 2021. Stratigraphic development of a late Oligocene reef complex under strong fluviatile influence in the Tertiary Piedmont Basin (Liguria, NW Italy). *Micropaleontology*, 67 (4): 315–339.

BROCCHI, G., 1814. *Conchiologia fossile subapennina con osservazioni geologiche sugli apennini e sul suolo adiacente.* Tomo Secondo. 241-712. Milano: Stamperia Reale.

BRONN, H. G., 1831. Übersicht der Fossilen Überreste in den tertiären subappeninischen Gebirgen. Italiens Tertirä-Gebilde und deren organische Einschlsüse. XII + 176 pp. Heidelberg.

CAHUZAC, B. and POIGNANT, A., 1997. Essai de biozonation de l'Oligo-Miocène dans les bassins européens à l'aide des grands foraminifères néritiques. *Bulletin de la Société Géologique de France,* 168: 155–169.

CAPPONI, G. and CRISPINI, L., 2002. Structural and metamorphic signature of alpine tectonics in the Voltri Massif (Ligurian Alps, North-Western Italy). *Eclogae Geologicae Helvetiae,* 95: 31–42.

CAPPONI, G., CRISPINI, L., FEDERICO, L., CABELLA, R., FACCINI, F., FERRARIS, F., FIRPO, M., MARESCOTTI, P., PIAZZA, M. and ROCCATI, A., 2013. Note illustrative al Foglio 212 'Spigno Monferrato' della Carta Geologica Regionale della Liguria, 114 pp. Regione Liguria, Dipartimento Ambiente: Genova, Italy.

CAPPONI, G., CRISPINI, L., FEDERICO, L. and MALATESTA, C., 2016. Geology of the Eastern Ligurian Alps: a review of the tectonic units. *Italian Journal of Geosciences,* 135: 157–169.

CAPPONI, G., CRISPINI, L., FEDERICO, L., PIAZZA, M. and FABBRI, B., 2009. Late alpine tectonics in the Ligurian Alps: constraints from the Tertiary Piedmont Basin conglomerates. *Geological Journal,* 44: 211–224.

CAPPONI, G., CRISPINI, L., PIAZZA, M. and AMANDOLA, L., 2001. Field constraints to the midtertiary kinematics of the Ligurian Alps. *Ofioliti,* 26: 409–416.

CAPPONI, G. and GIAMMARINO, S., 1982. L'affioramento oligocenico del Rio Siria (Bacino di Santa Giustina, provincia di Savona) nel quadro dei movimenti tardivi della Falda di Montenotte. *Atti della Società Toscana di Scienze Naturali, Memorie, Serie A,* 89: 101–113.

CHEN, X., ROMANIELLO, S. J., HERRMANN, A. D., WASYLENKI, L. E. and ANBAR, A. D., 2016. Uranium isotope fractionation during coprecipitationwith aragonite and calcite. *Geochimica et cosmochimica acta,* 188: 189–207.

D'ATRI, A., PIANA, F., TALLONE, S., BODRATO, G. and GASTALDI, M., 1997. Tettonica oligomiocenica nell'Alto Monferrato (Bacino Terziario Piemontese) e nel settore nord-occdentale del Gruppo di Voltri (Acqui Terme – Cassinelle, AL). *Atti Ticinensi di Scienze della Terra (Serie Speciale),* 5: 85–100.

DÈCHET, F., 1996. "Litostratigrafia e paleoecologia della scogliera oligocenica di case Cnè, (Dego -SV)." Unpublished master thesis, Università degli Studi di Genova, Genova, 100 pp.

DEFRANCE, M. J. L., 1822. Lenticulites. In: Cuvier, M. F., Ed., *Dictionnaire des Sciences naturelles,* 25 (laa-leo): 452-453. Strasbrourg et Le Normant, Paris: Levrault, F. G.,

EDER, W., BRIGUGLIO, A. and HOHENEGGER, J., 2016. Growth of Heterostegina depressa under natural and laboratory conditions. *Marine Micropaleontology,* 122: 27–43.

EDER, W., HOHENEGGER, J. and BRIGUGLIO, A., 2017. Depth-related morphoclines of megalospheric test of *Heterostegina depressa* d'Orbigny: biostratigraphic and palaeobiological implications. *Palaios,* 32: 110–117.

———, 2018. Test flattening in the larger foraminifer *Heterostegina depressa*: predicting bathymetry from axial sections. *Paleobiology,* 44: 76–88.

EHRENBERG, S. N., SVÅNÅ, T. A. and SWART, P. K., 2008. Uranium depletion across the Permian– Triassic boundary in Middle East carbonates: Signature of oceanic anoxia. *American Association of Petroleum Geologist Bulletin,* 92: 691–707.

FABRICIUS, K. E., DEATH, G., HUMPHREY, C., ZAGORSKIS, I. and SCHAFFELKE, B., 2013. Intraannual variation in turbidity in response to terrestrial runoff on near-shore coral reefs of the great barrier reef. *Estuarine, Coastal and Shelf Science,* 116: 57–65.

FEDERICO, L., CRISPINI, L., MALATESTA, C., TORCHIO, S. and CAPPONI, G., 2015. Geology of the Pontinvrea area (Ligurian Alps, Italy): structural setting of the contact between Montenotte and Voltri Units. *Journal of Maps,* 11: 101–113.

FEDERICO, L., CRISPINI, L., VIGO, A. and CAPPONI, G., 2014. Unravelling polyphase brittle tectonics through multi-software fault-slip analysis: the case of the Voltri Unit, Western Alps (Italy). *Journal of Structural Geology,* 68: 175–193.

FOSTER, G. J., ROYER, D. L. and LUNT, D. J., 2017. Future climate forcing potentially without precedent in the last 420 million years. *Nature communications,* 8: 14845.

GELATI, R. and GNACCOLINI, M., 1987. Sequenze deposizionali in un bacino episuturale nella zona di raccordo tra le Alpi ed Appennino settentrionale. *Atti Ticinensi di Scienze della Terra,* 31: 340–350.

GELATI, R., GNACCOLINI, M., POLINO, R., MOSCA, P., PIANA, F., MORELLI, M., FIORASO, G., BALESTRO, G., TALLONE, S. and RAMASCO, M., 2010. Note illustrative della carta geologica d'Italia alla scala 1: 50.000 - Foglio 211 "Dego", Litografia Geda, Italy, 124 pp.

GHIBAUDO, G., MASSARI, F., CHIAMBRETTI, I. and D'ATRI, A.R., 2014a. Oligo-miocene tectonosedimentary evolution of the Tertiary Piedmont Basin southern margin, Roccaverano area - Langhe sub-basin (NW Italy). *Journal of Mediterranean Earth Sciences,* 6: 1–51.

GHIBAUDO, G., MASSARI, F. and CHIAMBRETTI, I., 2014b. Oligo-miocene tectono-sedimentary evolution of the Langhe sub-basin: from continental to basinal setting (Tertiary Piedmont Basin - Northwestern Italy). *Journal of Mediterranean Earth Sciences,* 6: 53–144.

GIGLIA, G., CAPPONI, G., CRISPINI, L. and PIAZZA, M., 1996. Dynamics and seismotectonics of the West-Alpine arc. *Tectonophysics,* 267: 143–175.

GOETING, S., BRIGUGLIO, A., EDER, W., HOHENEGGER, J., ROSLIM, A. and KOCSIS, L., 2018. Depth distribution of modern larger benthic foraminifera offshore Brunei Darussalam. *Micropaleontology,* 64: 299–316.

GRADSTEIN, F.M., OGG, J.G. and SMITH, A.G., 2004. *A Geologic Time Scale 2004.* Cambridge: Cambridge University Press, 589 pp.

HOTTINGER, L., 1977. Foraminifères operculiniformes. *Mémoires Museum national d'Histoire naturelle, Série C - Sciences de la Terre,* 40:1-159, 66 plates.

KOCSIS, L., BRIGUGLIO, A., ROSLIM, A., RAZAK, H., CORIÆ, S. and FRIJIA, G., 2018. Stratigraphy and age estimate of Neogene shallow marine fossiliferous deposits in Brunei Darussalam (Ambug Hill, Tutong district). *Journal of Asian Earth Science,* 158: 200–209.

LEMOINE, P. and DOUVILLE, R., 1904. Sur le genre Lepidocyclina Gümbel. *Mémoire de la Socitété Géologique de France,* 32: 1–41.

LESS, G., 1991. Upper Oligocene larger Foraminifers of the Bükk Mountains (NE Hungary). *Annual Report of the Geological Institute of Hungary, 1989*, 411–465.

LESS, G., FRIJIA, G., ÖZCAN, E., SARASWATI, P. K., PARENTE, M. and KUMAR, P., 2018. Nummulitids, lepidocyclinids and Sr-isotope data from the Oligocene of Kutch (western India) with chronostratigraphic and paleobiogeographic evaluations. *Geodinamica Acta,* 30: 183–211.

LORENZ, C., 1969. Contribution a l'étude stratigraphique de l'Oligocène et du Miocène inferieur des confins liguro-piémontais. *Atti dell'Istituto di Geologia dell'Università di Genova,* 6: 273–889.

MCARTHUR, J.M., 1994. Recent trends in strontium isotope stratigraphy. *Terra Nova,* 6: 331–358.

MCARTHUR, J., M., HOWARTH, R. J. and BAILEY, T. R., 2001. Strontium isotope stratigraphy: LOWESS Version 3. Best-fit line to the marine Sr-isotope curve for 0 to 509 Ma and accompanying look-up table for deriving numerical age. *Journal of Geology,* 109: 155–169.

MCARTHUR, J.M., and HOWARTH, R.J., 2004. Sr-isotope stratigraphy: the Phanerozoic 87Sr/86Sr-curve and explanatory notes. In Gradstein, F.M., Ogg, J.G. And Smith, A.G., Eds., *A Geological Timescale 2004,* Chapter 7, pp. 96-102. Cambridge: Cambridge University Press.

MCARTHUR, J.M., HOWARTH, R.J. and SHIELDS, G.A., 2012. Strontium isotope stratigraphy. In: Gradstein, F.M., Ogg, J.G. And Smith, A.G., Eds., *A Geological Timescale 2004*, Chapter 7, pp. 127–144. Cambridge: Cambridge University Press.

MILLER, K. G., WRIGHT, J. D., FAIRBANKS, R. G., 1991. Unlocking the ice house: Oligocene–Miocene oxygen isotopes, eustasy, and margin erosion. *Journal of Geophysical Research: Solid Earth,* 96: 6829–6848.

MOSCA, P., POLINO, R., ROGLEDI, S. and ROSSI, M., 2010. New data for the kinematic interpretation of the Alps–Apennines junction (Northwestern Italy). *International Journal of Earth Sciences,* 99: 833–849.

MUTTI, E., PAPANI, L., DI BIASE, D., DAVOLI, D., MORA, S., SEGADELLI, S. and TINTERRI, R., 1995. Il Bacino Terziario Epimesoalpino e le sue implicazioni sui rapporti tra Alpi ed Appennino. *Memorie di Scienze Geologiche,* 47: 217–244.

O'BRIEN, C. L., HUBER, M., THOMAS, E., PAGANI, M., SUPER, J. R., ELDER, L. E. and, HULL, P. M., 2020. The enigma of Oligocene climate and global surface temperature evolution. *Proceedings of the National Academy of Sciences,* 117: 25302–25309.

ÖZCAN, E., LESS, G., BÁLDI-BEKE, M., KOLLÁNYI, K. and FERHAT, A., 2009. Oligo-Miocene Foraminiferal Record (Miogypsinidae; Lepidocyclinidae and Nummulitidae) from the Western Taurides (SW Turkey): Biometry and Implications for the Regional Geology. *Journal of Asian Earth Sciences,* 34: 740–760.

ÖZCAN, E., LESS, G., BÁLDI-BEKE, M. and KOLLÁNYI, K., 2010. Oligocene hyaline larger foraminifera from Kelereşdere Section (Muº, Eastern Turkey). *Micropaleontology*, 56: 465–493.

PAPAZZONI, C. A., COSOVIC, V., BRIGUGLIO, A. and DROBNE, K., 2017. Towards a calibrated larger foraminifera biostratigraphic zonation: Celebrating 18 years of the application of shallow benthic zones. *Palaios,* 21: 1-5.

PARENTE, M., and LESS, G., 2019. Nummulitids, lepidocyclinids and strontium isotope stratigraphy of the Porto Badisco Calcarenite (Salento Peninsula, southern Italy). Implications for the biostratigraphy and paleobiogeography of Oligocene Larger Benthic Foraminifera. *Italian Journal of Geosciences,* 138: 239–261.

PASQUARÈ, G., 1968, La Serie di Montenotte: un elemento alloctono sovrapposto al bacino oligocenico di Santa Giustina (Alpi liguri). *Rivista Italiana di Paleontologia e Stratigrafia,* 74: 1257–1273.

PECHEUX, M. J. F., 1995. Ecomorphology of a recent large foraminifer, Operculina ammonoides. *Geobios,* 28: 529–566.

QUARANTA, F., PIAZZA, M. and VANNUCCI, G., 2009. Climatic and tectonic control on the distribution of the Oligocene reefs of the Tertiary Piedmont Basin (NW Italy). *Bollettino della Societa Geologica Italiana,* 128: 587–591.

REUTER, M., PILLER, W. E., BRANDANO, M. and HARZHAUSER, M., 2013. Correlating Mediterranean shallow water deposits with global Oligocene–Miocene stratigraphy and oceanic events. *Global Planetary Change,* 111: 226–236.

SEDDIGHI, M., BRIGUGLIO, A., HOHENEGGER, J.and PAPAZZONI, C. A., 2015. New results on the hydrodynamic behaviour of fossil Nummulites tests from two nummulite banks from the Bartonian and Priabonian of northern Italy. *Bollettino della Società Paleontologica Italiana,* 54: 103–116.

SPAGNOLO, C., CRISPINI, L. and CAPPONI, G., 2007. Late structural evolution in an accretionary wedge: insights from the Voltri Massif (Ligurian Alps, Italy). *Geodinamica Acta,* 20: 21–35.

TORFSTEIN, A. and STEINBERG, J., 2020. The Oligo-Miocene closure of the Tethys Ocean and evolution of the proto-Mediterranean Sea. *Scientific Reports,* 10: 13817.

TORRES-SILVA, A. I., HOHENEGGER, W., CORIC, S., BRIGUGLIO, A. and EDER, W., 2019. Biostratigraphy and evolutionary tendencies of Eocene heterostegines in western and central Cuba based on morphometric analyses. *Palaios,* 32: 44–60

TORRES-SILVA, A. I., EDER, W., HOHENEGGER, W. and BRIGUGLIO, A., 2019. Morphometric analysis of Eocene nummulitids in western and central Cuba: taxonomy, biostratigraphy and evolutionary trends. *Journal of Systematic Palaeontology,* 17: 557–595

TRUEMAN, C. N. and TUROSS, N., 2002. Trace elements in recent and fossil bone apatite. *Reviews in Mineralogy and Geochemistry,* 48: 489–521.

ULLMANN, C. and KORTE, C., 2015. Diagenetic alteration in low-Mg calcite from macrofossils: a review. *Geological Quarterly,* 59: 3–20.

WIGNALL, P. B. and MYERS, K. J., 1988. Interpreting benthic oxygen levels in mudrocks: a new approach. *Geology,* 16: 452–455.

ZACHOS, J. C., DICKENS, G. R. and ZEEBE, R. E., 2008. An early Cenozoic perspective on greenhouse warming and carbon-cycle dynamics. *Nature,* 451: 279–283.

ZACHOS, J. C., FLOWER, B. P. and PAUL, H. A., 1997. Orbitally paced climate oscillations across the Oligocene/Miocene boundary. *Nature,* 388: 567–570.

APPENDIX 1
Species mentioned in the manuscript.

Eulepidina anatolica Özcan et al. 2010
Heterostegina sp. (Csokas)
Nephrolepidina morgani Lemoine and Douville 1904
Nummulites kecskemetii Less 1991
Operculina complanata (Defrance 1822)
Pecten arcuatus (Brocchi 1914)
Planoperculina complanata (Defrance 1822) *sensu* Hottinger 1977.
Pycnodonte brongniarti (Bronn 1831)

APPENDIX 2
Raw data counts on each thin section.

	CNE1.1	CNE1.2	CNE1.3	CNE2.1	CNE2.2	CNE2.3	CNE3.1	CNE3.2	CNE4.1
Bryozoa	iiiii	iiiii	iiiii		i	i	iiiiii	iiiiii	iiiiiii
Echinozoa	ii	iii			ii		iii	ii	i
Orbitoid	iii	iiii	iiiii				iiiiiiii	iiiiiii	iiiii
Red Algae	iiiiiiiiiiiiiii	iiiiiiiiiiiiiii	iiiiiiiiiii	iiii		iii	iiiiiiiii	iiiiiiiiiii	iiiiiii
SBF hyaline	iii	i		i		i			
SBF porcellaneous	i	ii						i	ii
SBF agglutinated									
Serpulid	i							i	
larger rotalid			i	ii		iiii		i	
Nummulites			i						
Amphistegenid			ii				iiii	ii	iii
Ostrid			ii					ii	ii
Coral				nearly all	nearly all	nearly all			
bivalve fragment					i	i		ii	ii
PF?						i			ii
Astigerina							i		
Operculina							i	ii	
ugly smaller benthic							iii	i	
dasy									i
balanid?							ii		i
Halimedacea									i
Alveolinid									
Gastropod									
Ostracod									
Spiroclypeus									
Acervulinid									

	CNE4.2	CNE4.3	CNE5	CNE6.1	CNE6..2	CNE6.3	CNE7	CNE7.2
Bryozoa	iiiiiiiiiiiiiiii	iiiiiiiiiii	iiiiiiii	iiiiiiiiiiiiii	iiiiiiiiiiiii	iiiiiiiiiiiiiiiii	iiiiiiiiiiiiiiii	iiiiiiiiiiiiii
Echinozoa	iiii	iiii	iii	iiii	iiii	iiii	iiiiiiiiiiiii	iiiiiii
Orbitoid	iiiiiiiiii	iiiiiiiiiiii	iiiiiiii	iiiiii	iiii	iiii	iiiiiiiiii	iiiiiiiii
Red Algae	iiiiiiiiii	iiiiiiiiiiii	iiiiiiiiiii	iiiiiiiiiiiiii	iiiiiiiiiiii	iiiiiiiiiiiiiiii	iiiiiiiiiiiiiiiiiii	iiiiiiiiiiiiiii
SBF hyaline	i			iii	iiiii	ii	i	iiiii
SBF porcellaneous	iiiiiii	iiiiii	iiii	ii	ii	i	iiiiii	iii
SBF agglutinated		i	ii	iiiiiii	iii	ii	iii	iiiiiii
Serpulid		ii	i		iii	iiii	i	
larger rotalid		iiii	iiiiiii	iiii	iii	i	ii	ii
Nummulites				i	i	iii	i	i
Amphistegenid	iiiii	iii	iiiiiii	iiiiiiii	iiiii	iiii	iiiiiiii	iiiiii
Ostrid	i			i			ii	i
Coral			i	ii	i			
bivalve fragment	iiii	iiiii	ii	iiiii	iiiii		ii	iiiii
PF?	ii			i				
Astigerina			ii	i	iii	i	iiiiiiiii	iiiiiiiii
Operculina	i		i	iiiii	iiiiii	iiii	iiiii	ii
ugly smaller benthic	i							
dasy								
balanid?		i						
Halimedacea	ii	ii		i	i	i		i
Alveolinid	iii	ii	i					
Gastropod				i	i			
Ostracod				i				
Spiroclypeus						i		
Acervulinid								i

	CNE8.1	CNE8.2	CNE9.1	CNE9.2	CNE9.3	CNE10.1	CNE10.2	CNE10.3
Bryozoa	i	ii	iii	ii	iiiii	i	iiiiii	iiii
Echinozoa	iii	iiiiiiii	iiiiiiii	iiiiiii	iiiii	iiii	iii	ii
Orbitoid	ii			i		i		i
Red Algae	iiiiiiiiiiiiiiiiiiiii	iiiiiiiiiiiiiiiiiiii	iiiiiiii	iiiiiiiii	iiiiiii	iiiii	iiiiiii	iii
SBF hyaline	iii	iiiiiiii	ii	i			i	
SBF porcellaneous	iiiiiii	iiiiiiiiii	iiiiii	iiii	ii	iiii	iii	
SBF agglutinated	iiiiiiiiii	iiiiiiiiiii	iii	iiiii	iiiii	iii	ii	i
Serpulid	i	iiii	i	ii	i	i		
larger rotalid	iii	ii	iiiiii	iiii	ii	iiii	iiii	i
Nummulites	ii	i						
Amphistegenid	i						i	i
Ostrid	ii							
Coral			i					
bivalve fragment	j	ii		i	i	i	i	ii
PF?	j	i						
Astigerina			i	i	i		ii	iii
Operculina		ii	i	i				
ugly smaller benthic								
dasy								
balanid?								
Halimedacea								
Alveolinid					i	i		
Gastropod								
Ostracod								
Spiroclypeus								
Acervulinid								